

AN EXAMINATION OF FROUDE-SUPERCritical FLOWS AND CYCLIC STEPS ON A SUBAQUEOUS LACUSTRINE DELTA, LAKE CHELAN, WASHINGTON, U.S.A.

AARON T. FRICKE,¹ BENJAMIN A. SHEETS,² CHARLES A. NITTRouer,¹ MEAD A. ALLISON,^{3,4} AND ANDREA S. OGSTON¹

¹*School of Oceanography, University of Washington, 1501 NE Boat Street, Seattle, Washington 98195, U.S.A.*

²*Barr Engineering, 4700 West 77th Street, #200, Minneapolis, Minnesota 55435, U.S.A.*

³*The Water Institute of the Gulf, One American Place, 301 North Main Street, Suite 2000, Baton Rouge, Louisiana 70805, U.S.A.*

⁴*Department of Earth & Environmental Sciences, Tulane University, New Orleans, Louisiana 70118, U.S.A.*

e-mail: atfricke@uw.edu

ABSTRACT: Density-driven submarine flows, including turbidity currents, play an important role in the transfer of sediment into deep water. These bottom-hugging flows often produce flow-transverse bedforms along their path. A sedimentological and geophysical survey of the Stehekin River delta in Lake Chelan, Washington, reveals a downslope-elongate field of bedforms on the delta foreset associated with hyperpycnal discharges of the Stehekin River. An analysis of the bedform morphologies, delta geometry, and density contrast between lake and river water suggests that these hyperpycnal flows are Froude-supercritical. The bedforms are likely cyclic steps, flow-transverse bedforms that are bounded by stable hydraulic jumps between alternating subcritical and supercritical flow regimes. The ability to examine the three-dimensional bed configuration produced by natural density-driven flows adds valuable information to the body of experimental work focused on the behavior of cyclic steps in flumes.

INTRODUCTION

Bedforms record valuable information about both the environments in which they were deposited and the nature of the flows under which they were formed. The dynamics of many bedforms, especially ripples and dunes, are well understood (see Ashley 1990 for review). Less well understood are bedforms produced under Froude-supercritical flows. A flow is Froude-supercritical when the wave speed at the flow interface exceeds the velocity of the flow. This balance is quantified in the case of subaqueous flows by the densimetric Froude number (Fr_d):

$$Fr_d = \frac{U}{\sqrt{\frac{\Delta\rho g}{\rho} D}} \quad (1)$$

where U is flow velocity, $\Delta\rho$ is the density contrast between the two water masses, g is gravitational acceleration, ρ is the density of the flow, and D is flow thickness (after Hand 1974). The critical densimetric Froude number is most often assumed to be unity. In open-channel flows, Froude-supercritical flows ($Fr > 1$) occur within a narrow band of conditions in which the flow is very thin and/or fast moving. By contrast, there is a wider range of flow conditions under which two-layer flows are likely to be supercritical. This is in large part due to the reduced density contrast at the flow interface which results in a slower interfacial wave speed (the denominator in Equation 1), yielding a higher densimetric Froude number.

Antidunes are a class of flow-transverse bedforms that occur under Froude-supercritical flow conditions. The surfaces of antidunes are in phase with the free surface of the flow (Kennedy 1963). Whereas antidunes are able to migrate both upstream and downstream, the former is more commonly observed. Upstream-migrating antidunes are generally

symmetric, with stoss and lee faces being of a similar angle. Antidunes are also described as ephemeral features that tend to grow, migrate, and collapse, only to regenerate in a different position, leaving little in the way of a clear sedimentary signature (Kostic 2011).

Cyclic steps are upstream-migrating bedforms that result from an alternating series of subcritical and supercritical flow regimes divided by steady, upstream-migrating hydraulic jumps. Fast-moving supercritical flow on the lee face of each step promotes erosion, while low-velocity flow following each hydraulic jump promotes sediment deposition on the stoss face, causing the bedforms to migrate in an upstream direction (Parker 1996; Kostic et al. 2010; Kostic 2011).

Classic experimental work by Hand (1974), as well as more recent studies by Winterwerp et al. (1992), Kostic et al. (2010), and Cartigny (2012) have explored bedforms produced by supercritical density currents in laboratory environments. Fewer studies have explicitly described supercritical bedforms in nature (e.g., Fildani et al. 2006; Lamb et al. 2008; Covault et al. 2014), but many studies suggest the predominance of cyclic-step-related bedforms in submarine environments, including the sediment waves common in many continental-slope environments (e.g., Kostic 2011; Cartigny 2012). These field examples come from marine environments, where energetic forces (waves, tides, currents) are likely to affect both flows and the resultant bedforms, thus making their formative mechanisms difficult to isolate.

Here we present data from a comparatively quiescent environment, the subaqueous delta of the Stehekin River in Lake Chelan, Washington, USA. Satellite and aerial images of the mouth of the Stehekin River during high-flow conditions suggest that the discharge of the river plunges, as evidenced by buoyant debris marking a plunge point and the absence of any surface plume spreading lakeward (Fig. 1). Geophysical and sedimentological data sets show a kilometer-scale train of bedforms

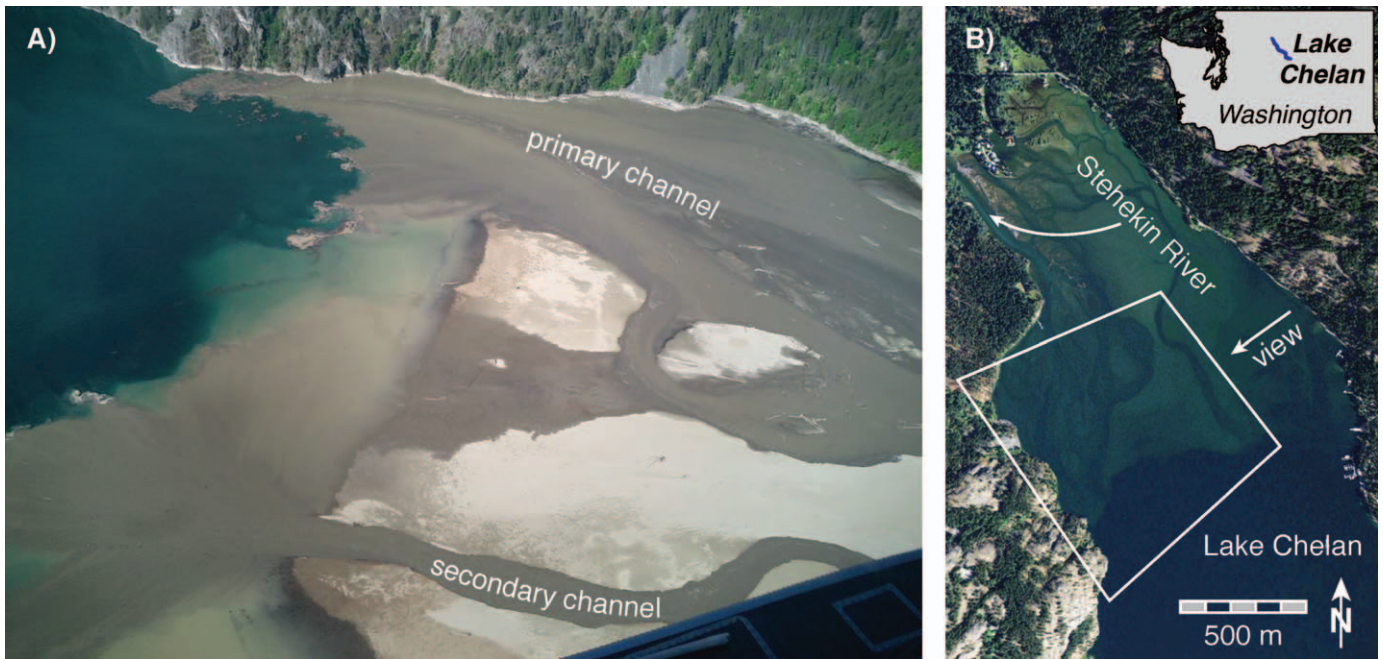


FIG. 1.—A) Photograph looking southwest across the Stehekin River delta during a flood ($\sim 300 \text{ m}^3 \text{ s}^{-1}$) on 18 May 2006. Flow is confined to a primary channel along the western edge of the delta topset, and a smaller secondary channel farther to the east. The flow completely plunges within 200 m of the delta rollover. Buoyant woody debris marks the edge of the hyperpycnal plume originating from the western topset channel. Photo courtesy of Vince Ward and golakechelan.com. B) Satellite image of the Stehekin River delta showing the approximate limits of the photo in Part A. Satellite image taken 10 August 2012, courtesy of the USDA Farm Service Agency via Google Earth.

that appear to be cyclic steps on the foreset of the delta. Our objectives are to: (1) describe the physical setting of these bedforms, (2) determine whether hyperpycnal discharges from the Stehekin River are Froude-supercritical, (3) determine the bedform type based on geometry and stability in estimated flow conditions, (4) link bedform formation to the dynamics of the Stehekin River, and (5) relate flow dynamics to the planform characteristics of the bedform field.

STUDY AREA

Lake Chelan

Lake Chelan is located in the northeastern Cascade Range of Washington State. It occupies a long, narrow valley of glacial origin (Whetten 1967). The lake is approximately 80 km long, with an average width of roughly 2 km. Lake Chelan has a maximum depth of 450 m (50 m below sea level), though much of the lake is shallower, with an average depth of ~ 150 m. Lake level fluctuates by approximately 3 m annually due to outflow regulation for hydroelectric-power generation.

Lake Chelan is a cold, oligotrophic lake (Pelletier et al. 1989) (Fig. 2). The temperature of lake water below 100 m depth remains $\sim 6^\circ \text{C}$ throughout the year. Surface warming during the summer months results in strong stratification from May through December, with a thermocline at a depth of ~ 70 m (Pelletier et al. 1989).

Stehekin River

The Stehekin River enters the northern end of Lake Chelan, near the village of Stehekin, Washington. It drains 830 km² of mountainous, seasonally snow-covered terrain. Nearly all of the Stehekin River watershed lies within the boundaries of North Cascades National Park or the Lake Chelan National Recreation Area. As a result, the watershed has been preserved in a relatively natural condition. The typical Stehekin River hydrograph is characterized by an extended spring freshet

(May–July) and intense, short-lived, late-fall discharge events (Fig. 2). Average discharge of the Stehekin River is $40 \text{ m}^3 \text{ s}^{-1}$, with peak flood discharges up to an order of magnitude greater. While numerous small streams enter Lake Chelan, the Stehekin River is the dominant source of water and sediment to the northern part of the lake.

METHODS

Field

Sedimentological and geophysical data were collected during June 2010 in the northern five kilometers of Lake Chelan near the Stehekin River delta. Kasten-style gravity cores (Kuehl et al. 1985) and Shipek surface grab samples were collected in water depths greater than 50 m (Fig. 3) using a modular coring barge. Shallow-water grab samples were collected from a small aluminum skiff. All geophysical data were collected using the R/V Lake Itasca (University of Texas Institute for Geophysics).

Geophysical Data

Multibeam bathymetric data were acquired using a 512-beam Reson SeaBat 7101 system mounted to the R/V Lake Itasca. These data were processed using CARIS software to produce a bathymetric surface (Fig. 4). Lake Chelan sits in a narrow and steep-sided basin in which GPS satellite reception is poor, and some associated artificial noise remains in the final bathymetric surface, such as NW–SE lineation in deeper water, and NE–SW lineation on the delta top (Fig. 4). Fifty kilometers of subbottom CHIRP (Compressed High Intensity Radar Pulse) profiles were collected using an EdgeTech SB216-S towfish operating with a pulse-frequency range of 2–16 kHz. Penetration and resolution varied throughout the survey area due to differences in sediment types and particularly the amount of biogenic gas in the sediment, which severely impeded imaging in the deepest parts of the lake.

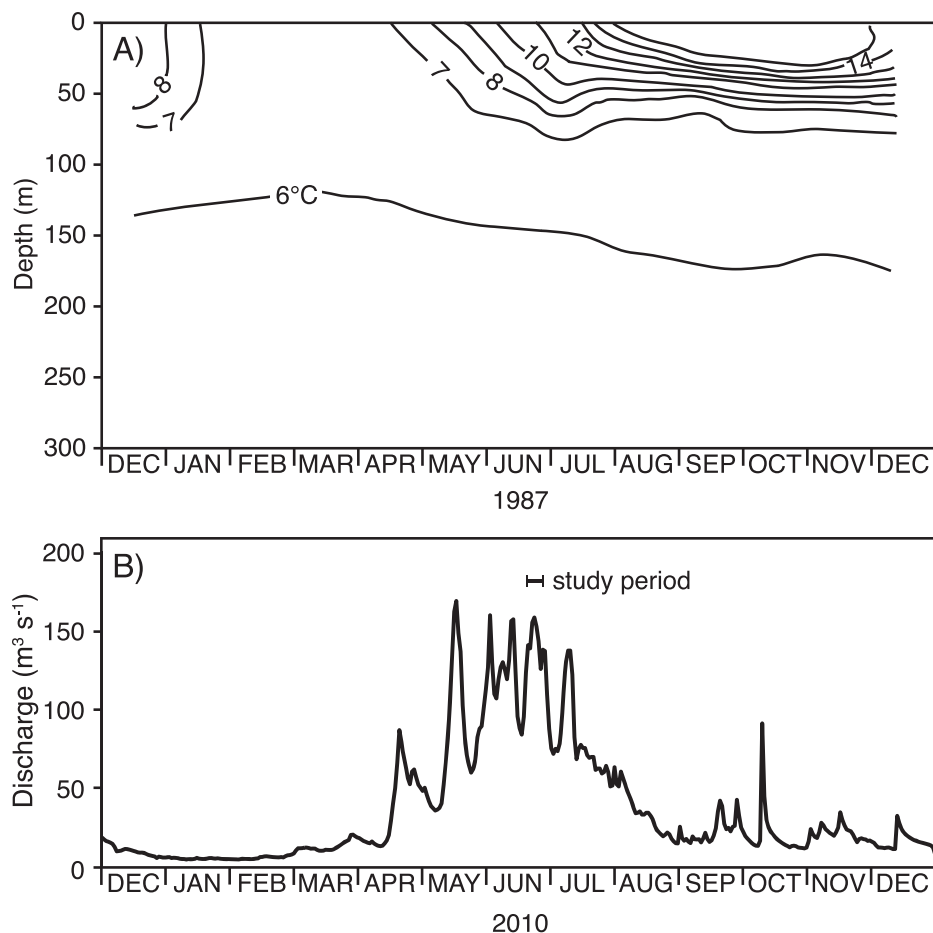


FIG. 2.—Hydrography of Lake Chelan and the Stehekin River. **A)** Time series showing the thermal structure of the northern basin of Lake Chelan in 1987, isotherms from Pelletier et al. (1989). **B)** Discharge of the Stehekin River in the year 2010, data from USGS gauge on the Stehekin River (#12451000).

Core Processing

Kasten cores were opened and processed in the field. A 2-cm-thick slab was removed along the length of each core, and the slabs were X-rayed in the laboratory using a digital X-ray system. The remainder of each core was cut into 2-cm intervals and bagged for radiochemical and grain-size analyses. Grain-size distributions of the mud fraction from each sample ($<64 \mu\text{m}$) were determined using Micromeritics Sedigraph 5100 and 5120 particle size analyzers. Grain-size distributions of the sand fraction from each sample were determined using a two-meter-tall automated settling column.

Sediment accumulation rates were determined using the procedure outlined by Nittrouer et al. (1979) in which ^{210}Pb activities are determined by measuring the activity of its granddaughter, ^{210}Po , relative to a calibrated spike of ^{209}Po . ^{210}Pb has a half-life of 22.3 years, and can be used to constrain sediment accumulation over the past century. Sediment accumulation rates were calculated by solving:

$$S = \frac{\lambda z}{\left(\frac{A_0}{A_z}\right)} \quad (2)$$

where S is the sediment accumulation rate, λ , is the decay constant for ^{210}Pb , A_0 and A_z are excess ^{210}Pb activities at two points within the region of log-linear decay, and z is the difference in depth between A_0 and A_z .

RESULTS

Delta and Basin Morphology

The bathymetric survey reveals a narrow steep-sided basin that is being filled symmetrically by the prograding Stehekin River delta. Two channels cross the delta topset, each of which is connected to the river at its landward extent (Fig. 3). The primary (western) channel is wider and deeper than the secondary channel, and appears to carry much of the discharge during flood events (Fig. 1). The break in slope between the delta topset and foreset (i.e., the rollover) was found at a depth of $\sim 12 \text{ m}$ at the time of this study. The upper 200 m of the foreset (measured along dip) is relatively steep ($\sim 7^\circ$), and the lower foreset averages 3° (Fig. 5A). The glacially scoured sidewalls of the lake are universally steep, and in the southern end of the study area exceed 45° . Multiple small streams enter the lake from its east and west sides, but the contribution of sediment from these sources to the study area is negligible. Although the sidewalls and delta foreset are locally steep, there is evidence of only one slump feature, on the west margin of the lake, which has a surface area $\sim 15,000 \text{ m}^2$.

Bedforms

Bedforms originate on the steep part of the upper foreset near the slope break and extend 1300 m downlake into water depths $> 115 \text{ m}$ (Figs. 5A, 6). The bedforms have sinuous crests and are composed of well-sorted fine

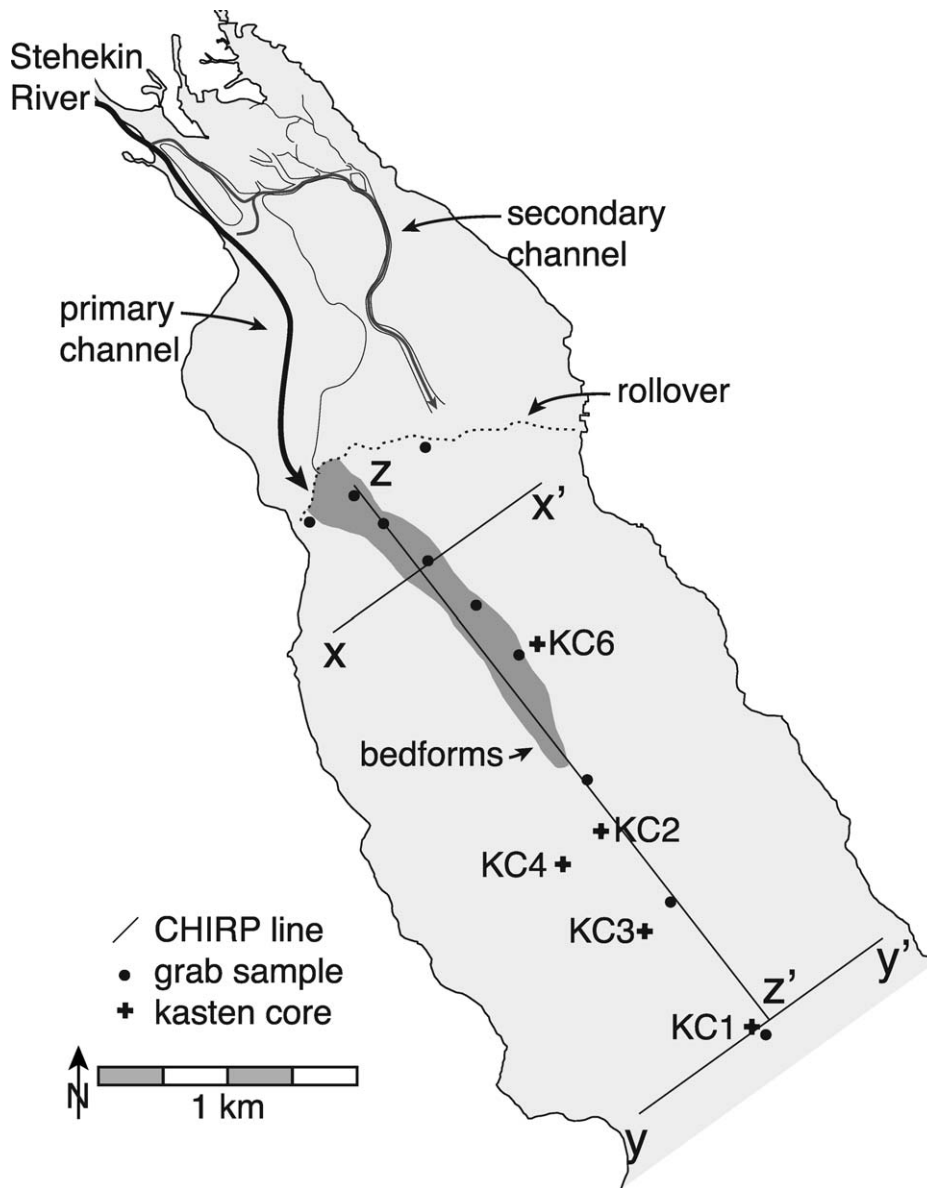


FIG. 3.—Map of the study area showing major geomorphic features, sample locations, and CHIRP survey lines. The primary and secondary topset channels connecting the Stehekin River to the delta rollover are marked by black and gray arrows, respectively. The delta rollover is marked by a dotted line, and the bedform field is marked by dark gray shading. Letters marking the ends of CHIRP lines (e.g., X–X') reference CHIRP lines shown in Figure 5.

sand ($D_{50} = 2.8 \phi$; $150 \mu\text{m}$). The most proximal bedforms have an amplitude of ~ 2 m and a wavelength of ~ 20 m, with bedform wavelength increasing toward the distal limit of the bedform field, as determined from the CHIRP line in Figures 5A and 6. These bedforms occur as a bathymetric high relative to the surrounding lake bottom. This is in contrast to bedforms found in many other natural settings (e.g., rivers, continental slopes), where bedforms occur within obvious channel bathymetry. There is no evidence of local channelization or levee topography associated with the bedform field in Lake Chelan (Fig. 5B).

Grain Size

Sediment on the delta foreset is divided into four grain-size populations on the basis of position on the foreset (Fig. 7). Samples collected along a 900-m transect down the axis of the bedforms are well sorted, with a mean diameter (D_{50}) of 2.8ϕ ($150 \mu\text{m}$). This stands in contrast to sediment collected ~ 200 m off axis of the proximal limit of the bedform field, which is much finer ($D_{50} = 6.1 \phi$; $14 \mu\text{m}$). The off-axis sediment has a distribution of grain sizes similar to sediments collected beyond the distal limit of the

bedforms. The bedforms are not apparent in either the multibeam or CHIRP datasets beyond ~ 1300 m down the foreset. The three samples collected downlake of the bedforms become finer toward the distal end of the system from $D_{50} = 5.0 \phi$ ($31 \mu\text{m}$) to $D_{50} = 6.6 \phi$ ($10 \mu\text{m}$). Cores from intermediate positions on the foreset (KC2, KC3, and KC4) (Fig. 4) show little variability within the finer-grained sediment below 20 cm. The most proximal and most-distal cores (KC6 and KC1, respectively) show considerably more variability in grain size below 10–20 cm (Fig. 8).

Sediment Accumulation Patterns

Sediment accumulation rates determined via ^{210}Pb analysis of the kasten cores are generally greatest in the proximal part of the basin (KC2: 0.50 cm y^{-1}) and diminish with increasing distance from the Stehekin River mouth (KC1: 0.34 cm y^{-1}) (Fig. 9). Sediment accumulation rates from KC2 and KC4, both of which were collected at a similar distance from the delta rollover, show a decrease in the rate of sediment accumulation toward the lateral margin of the lake. The most proximal core, KC6, does not show the highest accumulation rate, but similar to

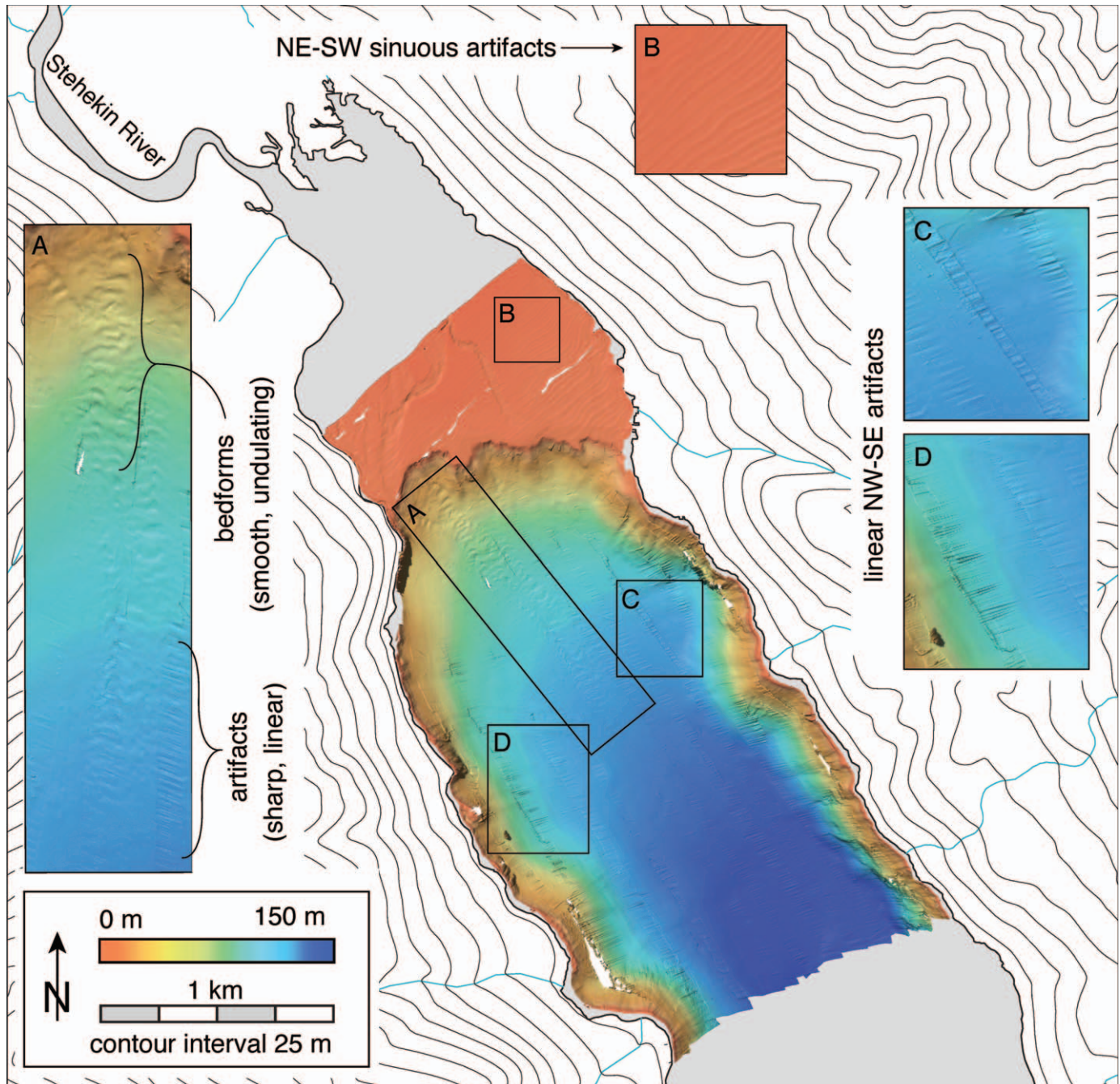


FIG. 4.—Bathymetric chart of the northern 5 km of Lake Chelan. The Stehekin River enters the north end of the lake where it builds a delta. Bathymetry is shown over a USGS basemap. Insets A–D identify selected artifacts in the bathymetric surface and features interpreted to be bedforms.

KC4, it was collected more toward the lateral margin of the lake. Plots of excess ^{210}Pb from all cores exhibit steady-state log-linear decay ($R^2 = 0.76\text{--}0.97$) from the bottom of each core to within 10–20 cm of the surface. Excess ^{210}Pb activities in the upper 10–20 cm of each core are uniform and low relative to activities directly below this interval.

DISCUSSION

The most noticeable feature on the foreset of the Stehekin River delta is the elongate field of bedforms that runs from the uppermost foreset ~1300 m along the lake floor to a depth exceeding 100 m. We hypothesize

that these bedforms are the product of hyperpycnal flows originating from the Stehekin River. In the following discussion, we characterize the type of density-driven flows acting in this system, classify the bedforms, and relate flow conditions to both the upstream fluvial system and the sedimentary signals preserved in lake-bed sediment.

Froude-Supercritical Flows

The bedforms on the foreset of the Stehekin River delta occur between ~60 m and ~115 m water depth. At these depths no surface-wave energy reaches the lake bed, and the lacustrine setting precludes any powerful

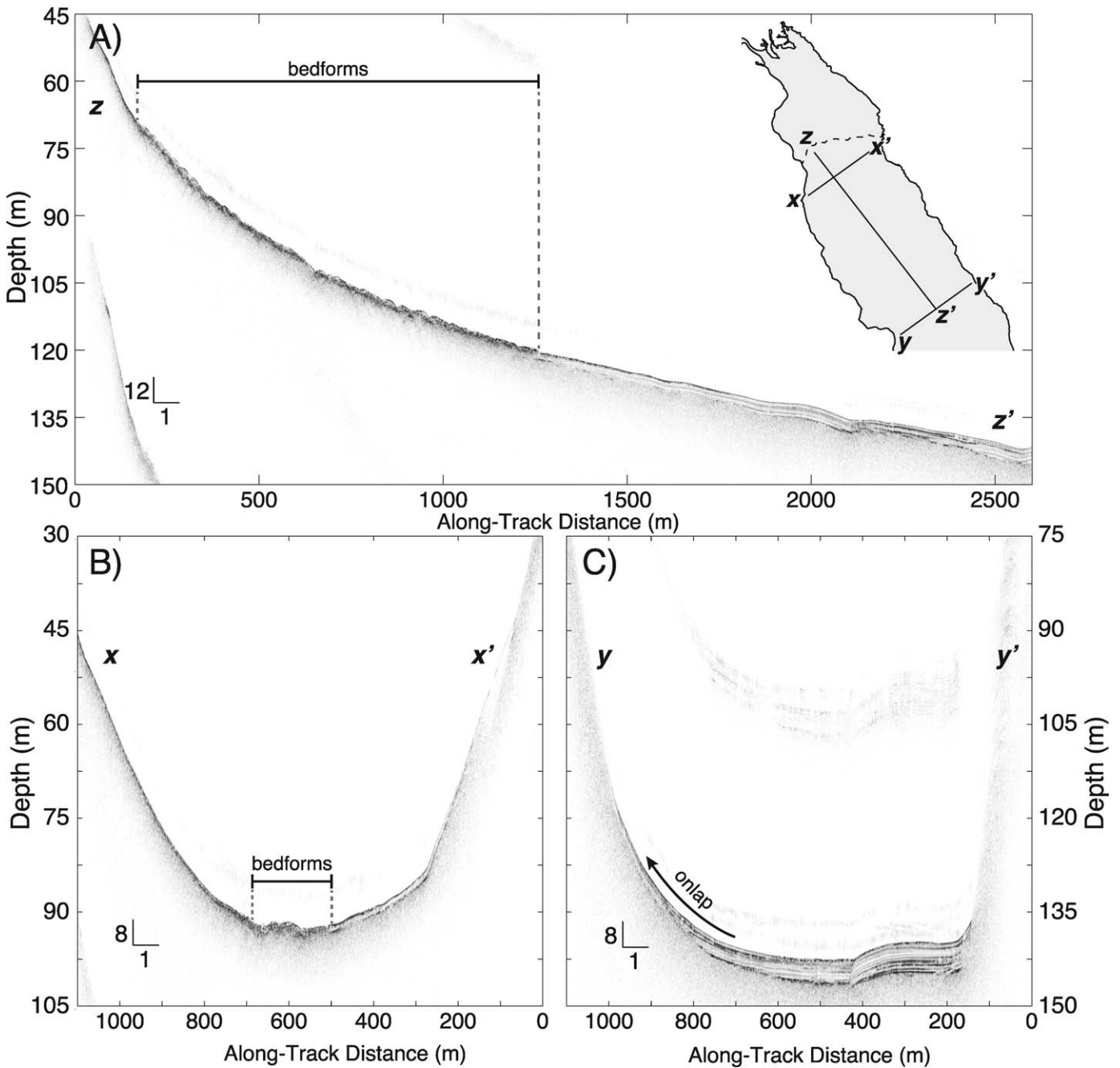


FIG. 5.—Three CHIRP profiles from the foreset of the Stehekin River delta. An inset in Part A shows the location of each profile and a dashed line marking the delta rollover. The vertical axis in each plot is depth in meters calculated from two-way travel time assuming a sound velocity of 1500 m s^{-1} . Limited penetration of the CHIRP signal is due primarily to biogenic gas in the sediment. **A)** Profile extending 2600 meters along the axis of the lake. The bedforms are marked by undulating bathymetry. **B)** Proximal cross-lake profile. Note the elevated bedforms. **C)** Distal cross-lake profile, which exhibits reflectors that onlap the steep sides of the basin, a relationship common in the distal portion of the study area.

currents as would be common in the marine environment. Consequently, the bedforms must be formed by bottom-hugging flows moving down the foreset of the Stehekin River delta. Because of the steep slope of the foreset, any such flow will be Froude-supercritical. The dependence of the densimetric Froude number on slope is evident by substituting an equation for the velocity of a density current into the densimetric Froude number equation (Eq. 1), for example the modified version of the Chézy Equation described by Kneller and Buckee (2000):

$$\bar{U} = \sqrt{\frac{8g \frac{\Delta\rho}{\rho} SD}{f_b + f_i}} \tag{3}$$

where \bar{U} is density-current velocity, g is gravity, S is slope, D is flow thickness, and f_b and f_i are Darcy-Weisbach friction coefficients at the top and bottom interfaces of the flow, respectively. Substituting Equation 3 into Equation 1 and simplifying, yields the densimetric Froude number (Fr_d):

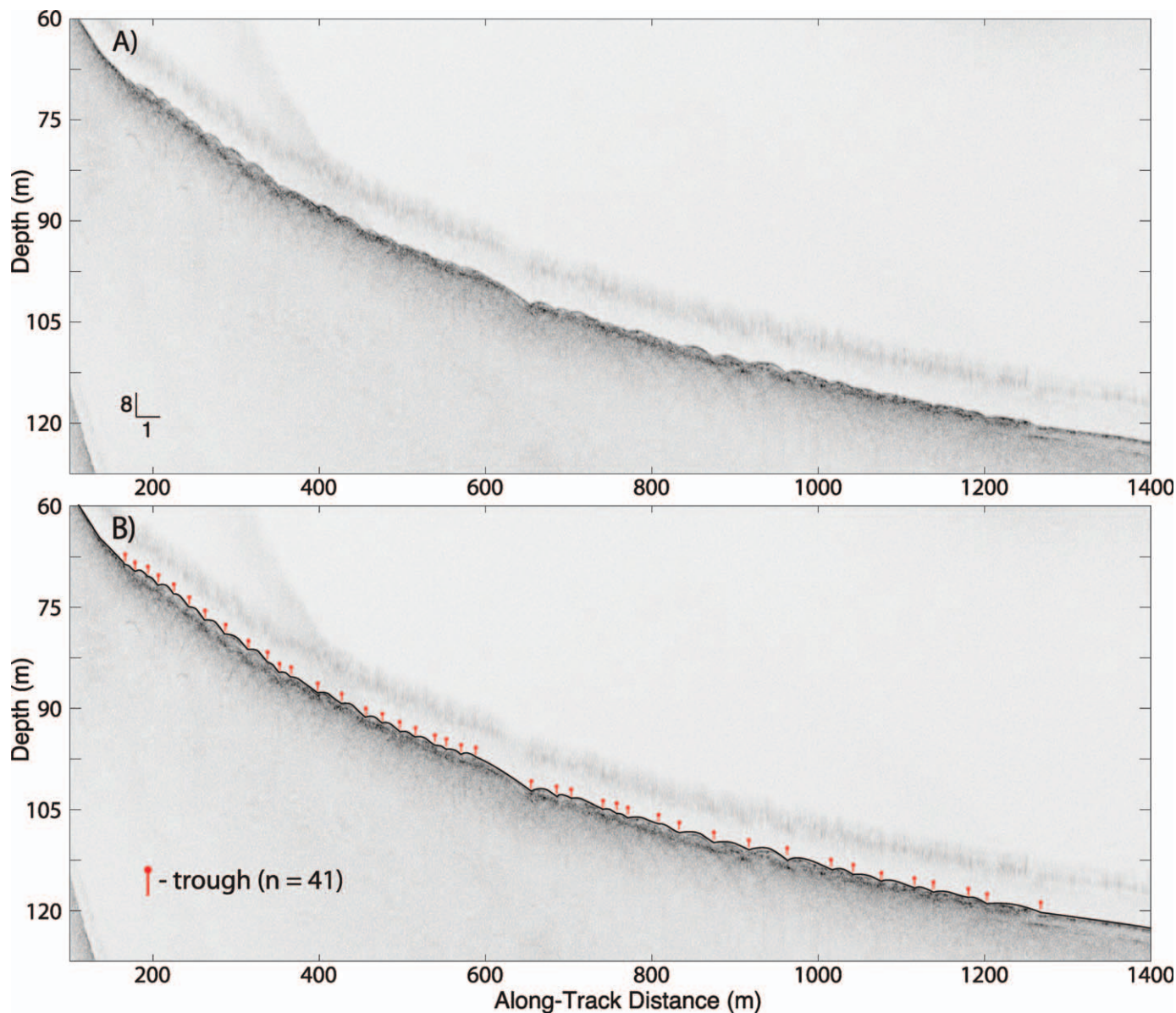


FIG. 6.—Raw and annotated CHIRP profile through the bedform field on the foreset of the Stehekin River delta. The position of the bedforms on the foreset is noted in Figure 5. The vertical axis in each plot is depth in meters calculated from two-way travel time assuming a sound velocity of 1500 m s^{-1} . **A)** Raw CHIRP profile showing the bedforms and the transition to flat-lying sediments marked by parallel reflectors at $\sim 1300 \text{ m}$ distance. **B)** Annotated copy of the CHIRP line in panel Part A showing the bedform–water interface traced with a black line, and the location of 41 bedform troughs marked with red flags.

$$Fr_d = \sqrt{\frac{8S}{f_b + f_i}} \quad (4)$$

Middleton and Southard (1984) suggest using a value of 0.01 for the summed Darcy-Weisbach friction coefficients ($f_b + f_i$) for large turbidity currents. This modified formulation of the densimetric Froude number is also described by Hand (1974), who suggests that the Darcy-Weisbach friction coefficients usually sum to ~ 0.057 based on experimental results. Using suggested Darcy-Weisbach friction coefficients from Middleton and Southard (1984) and Hand (1974) as endmembers, the critical slope needed to produce a Froude-supercritical flow is between 0.00125 (0.07°) and 0.007 (0.40°), respectively. Because the slope of the bedform field on the

Stehekin River delta is generally > 10 times steeper than such critical slopes, bottom-hugging flows will be Froude-supercritical in this system.

Antidunes versus Cyclic Steps

Antidunes and cyclic steps are the bedforms produced under Froude-supercritical flow conditions (e.g., Kennedy 1963; Hand 1974; Taki and Parker 2005; Sun and Parker 2005; Kostic et al. 2010; Cartigny 2012). Antidunes and cyclic steps share a number of attributes, and distinguishing between the bedforms is challenging. The stratification geometry of the two types is distinct, but we are unable to resolve sufficient detail in our CHIRP data to distinguish between them (Fig. 5). However, it is possible to determine whether antidunes or cyclic steps could form in this setting by

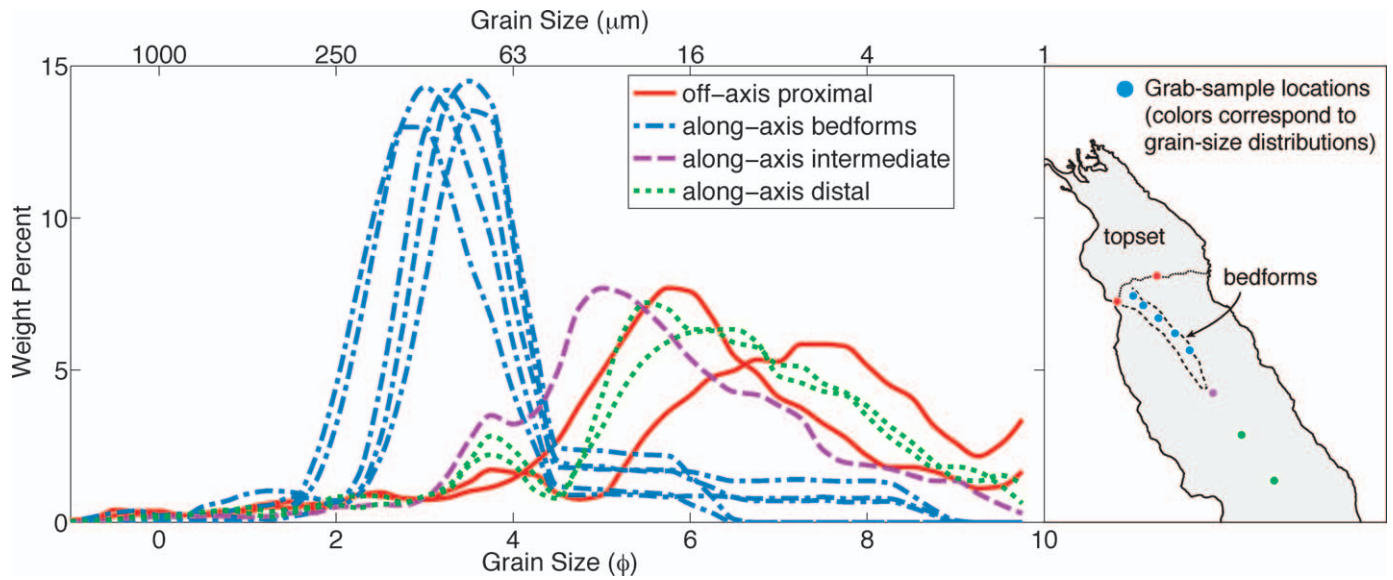


FIG. 7.—Grain-size distributions of 10 surface grab samples collected on the foreset of the Stehekin River delta. Distributions have been divided into four populations based on foreset location. Map on right shows the locations of samples. Red solid lines correspond to grab samples collected ~ 200 m off-axis at the proximal end of the bedform field. Blue dot-dashed lines correspond to samples along a 900-m-long transect through the bedform field. The purple dashed line corresponds to a sample collected inline with the bedforms, but farther downlake. Green dotted lines correspond to samples also collected inline with, but substantially downlake of, the bedforms.

constraining the flow velocities associated with each type of bedform. The flow speed over antidunes is equal to the celerity of a wave of the same wavelength as the antidunes (Hand 1974). In this case, the interface between the flow and the overlying ambient water is in phase with the bed (i.e., the upper surface of the density current is in phase with the undulations of the antidunes). This wave at the upper interface of the flow, and the antidunes below it, are held nearly stationary because the interfacial wave propagates upstream at approximately the same speed as the flow moves downstream. Flow velocity is therefore related to antidune wavelength by

$$\bar{U} = \sqrt{\frac{gL}{2\pi} \frac{\Delta\rho}{\rho + \rho'}} \tag{5}$$

where \bar{U} is the mean current velocity, g is gravitational acceleration, L is the wavelength of bedform, $\Delta\rho$ is the density contrast across the interface, ρ is the density of the flow, and ρ' is the density of the ambient fluid (Hand 1974). A range of solutions to Equation 5 are calculated using a bedform wavelength of 25 m (mean of the 40 bedforms measured from CHIRP data) (Fig. 10). Such flow velocities are too slow to be realistic, given the steep slope of the

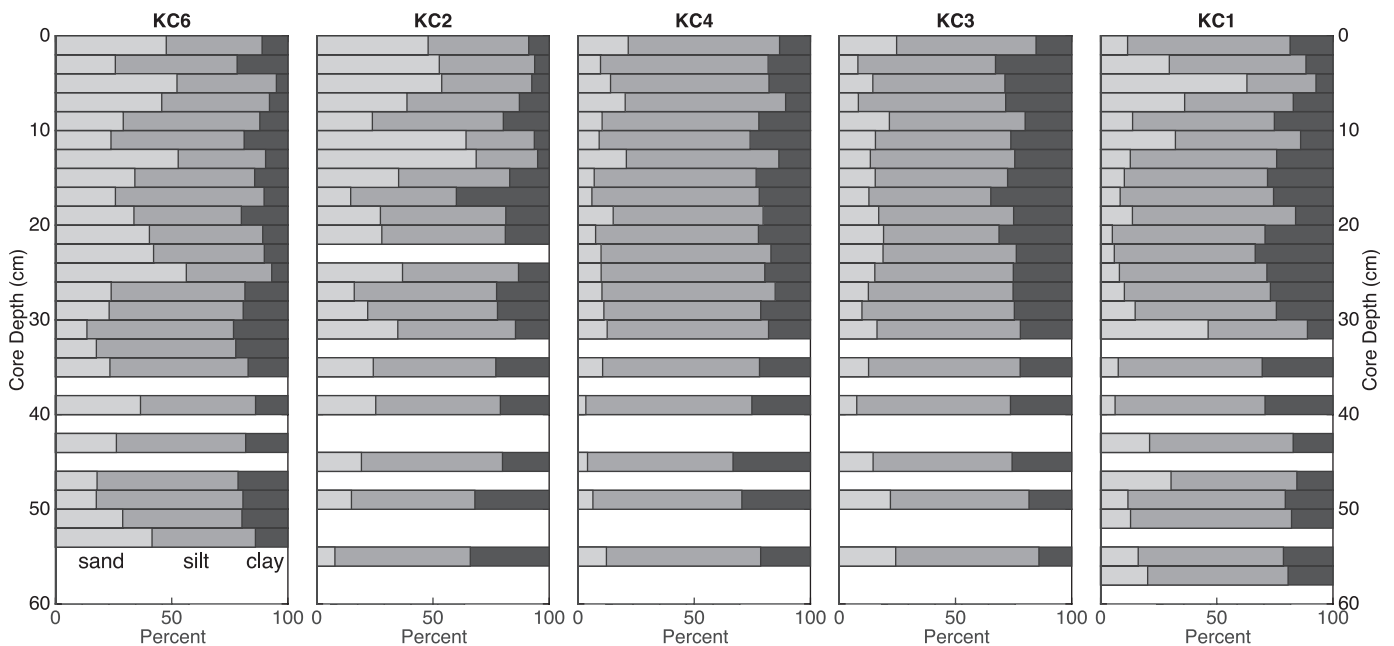


FIG. 8.—Sediment grain size over the lengths of five kasten cores. Plots are arranged from most proximal (left) to most distal (right) (see Fig. 3). Percent sand (light gray), silt (medium gray), and clay (dark gray) are shown for selected 2-cm intervals.

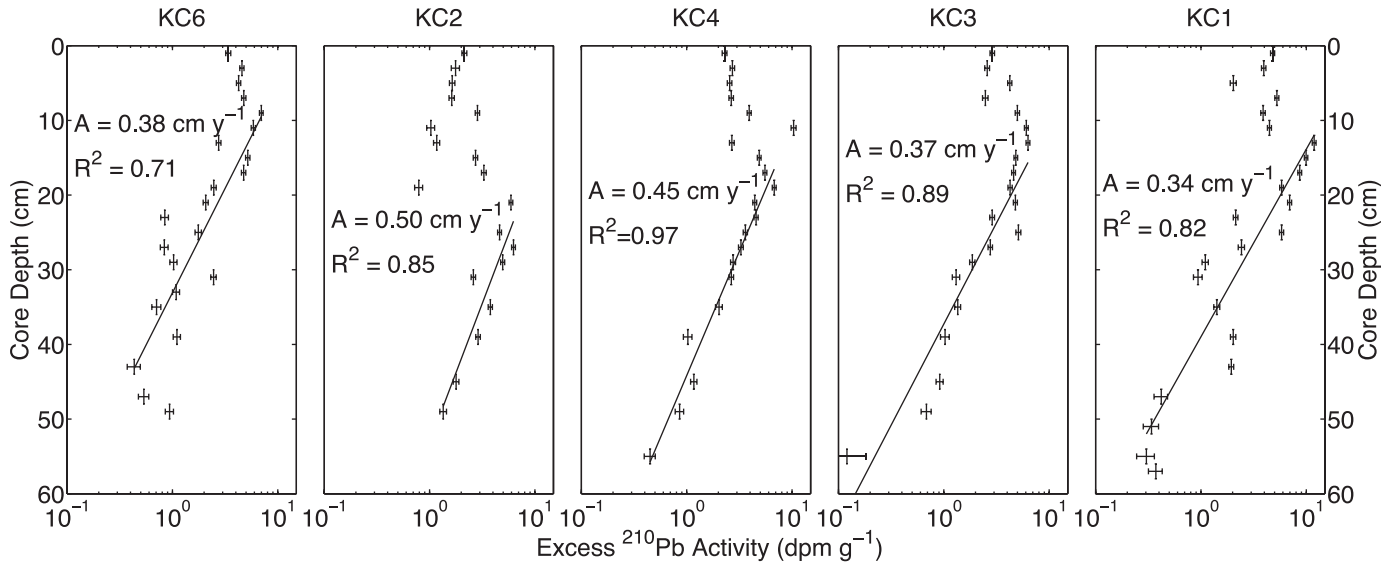


FIG. 9.—Excess ²¹⁰Pb activity from five kasten cores. Panels are arranged from most proximal (left) to most distal (right) (see Fig. 3). Log-linear regressions and correlation coefficients are determined for the region of log-linear decay.

delta foreset, as shown by solving Equation 3 using the average slope (S) of the bedform field of 5° , a flow thickness (D) of 2.5 m, and a range of summed Darcy-Weisbach friction coefficients ($f_b + f_i$) between 0.010 and 0.057. Such solutions show that the flow velocities expected on the foreset exceed the velocities that are compatible with antidunes of the observed wavelength (Fig. 10). A flow thickness of 2.5 m was chosen based on estimates from

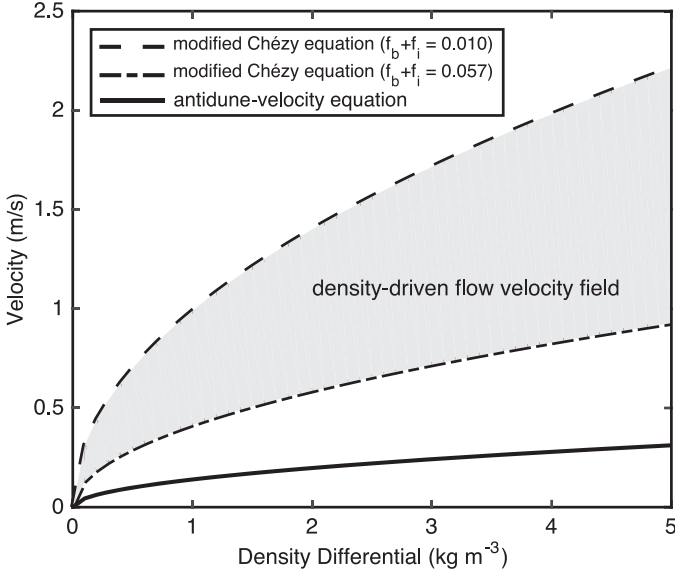


FIG. 10.—Three relationships between excess density and velocity for hyperpycnal flows given a bedform wavelength of 25 m. The solid line is a solution to Equation 5 from Hand (1974), which is independent of flow depth, and assumes the bedforms are antidunes. The dashed line is a solution to Equation 3 given a hyperpycnal flow thickness of 2.5 m, and summed Darcy-Weisbach friction coefficients ($f_b + f_i$) of 0.010. The dot-dash line is a solution to Equation 3 given a hyperpycnal flow thickness of 2.5 m, and summed Darcy-Weisbach friction coefficients ($f_b + f_i$) of 0.057. The shaded region represents the range of possible density-driven flow velocities given summed Darcy-Weisbach friction coefficients ($f_b + f_i$) between the experimental value of 0.057 (Hand 1974) and the value of 0.010 for large turbidity currents from Middleton and Southard (1984).

Kostic (2011) that suggest the ratio of cyclic step wavelength to flow thickness is ~ 10 . The wavelength of antidunes would need to be ~ 10 times the observed bedform wavelength in order to produce an upstream-propagating interfacial wave with a celerity sufficiently high to balance the downstream flow velocities expected to occur on the steep foreset. Based on these relationships, we posit that the bedforms on the foreset of the Stehekin Delta are cyclic steps.

Morphology of Cyclic Steps

The morphology of cyclic steps has been explored in flume experiments, where external forces common in natural environments (e.g., waves, currents, tides) are eliminated. Recent work by Spinewine et al. (2009), Kostic et al. (2010), and Cartigny (2012) has characterized the development and evolution of cyclic steps in laboratory experiments. Fortunately, in the relatively quiescent environment of Lake Chelan, such external forces are also negligible, allowing the attribution of sedimentary signatures to hyperpycnal flows, which permits straightforward comparison with these experimental studies.

Spinewine et al. (2009) report an upward-concave profile in the experimental slope on which cyclic steps are observed. This upward-concave profile is also a characteristic of sediment wave fields according to Lee et al. (2002), which in most cases are likely cyclic steps (Spinewine et al. 2009; Kostic et al. 2010). The longitudinal profile through the bedform field on the foreset of the Stehekin delta is similarly concave upward (Fig. 5A).

The cyclic steps on the foreset of the Stehekin delta were imaged in both the bathymetric and CHIRP datasets. Because artifacts in the multibeam bathymetry interrupt any continuous line along the length of the bedform field, we have chosen to measure bedform wavelengths from a single CHIRP line (Fig. 6). Measurements from the 40 bedforms along this CHIRP line show cyclic-step wavelength increases with distance from the rollover between delta topset and foreset (Fig. 11B). For this analysis, the wavelength of each bedform is defined as the distance between adjacent troughs (Fig. 6B). The P-value of the regression is very small ($P = 0.0001$), indicating a significant relationship between bedform wavelength and distance from the delta rollover. This relationship is consistent with prediction, assuming that the bedforms are cyclic steps.

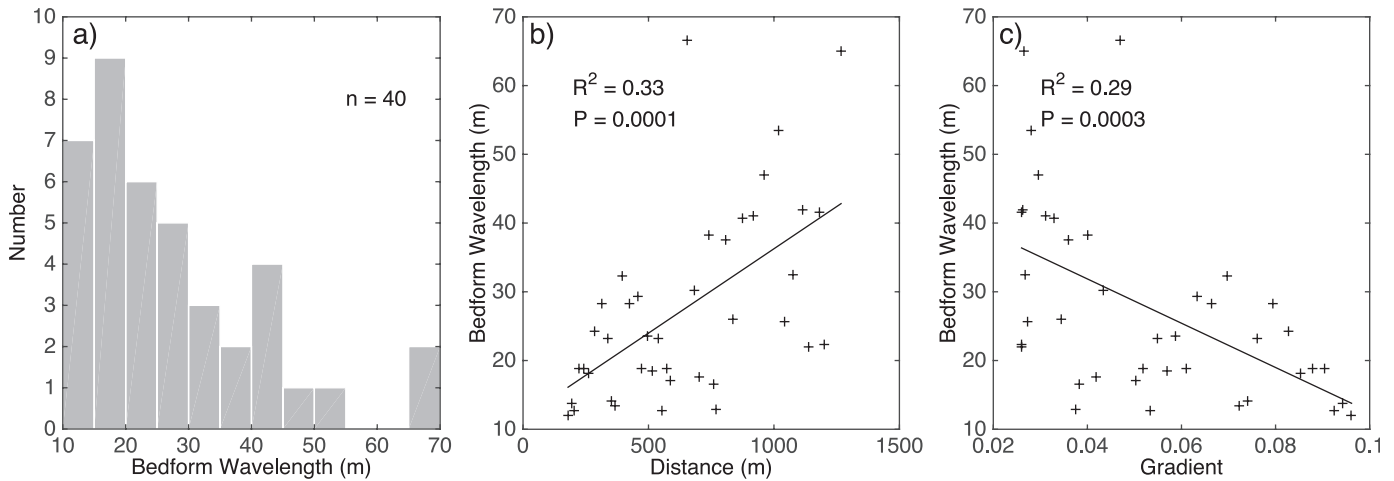


FIG. 11.—Relationship between bedform wavelength and setting on the delta foreset. Bedform wavelengths, distances, and foreset gradient were derived from CHIRP data collected in the bedform field (Fig. 6). **A)** Histogram of the wavelengths of the 40 bedforms imaged in the CHIRP line shown in Figure 6. Wavelengths have been placed into 5-m bins. **B)** Bedform wavelength with respect to distance down the foreset from the delta rollover. **C)** Bedform wavelength with respect to local foreset gradient centered at each bedform.

In the proximal part of the bedform field, both the steep gradient of the bed and the excess density of the flow promote rapid acceleration and destabilization of the flow, yielding tightly spaced hydraulic jumps. In the more distal part of the bedform field, where the gradient is decreased and mixing reduces the excess density of the flow, the acceleration and destabilization of the flow requires greater distance, yielding cyclic steps spaced farther apart. The observed relationship between local foreset gradient and bedform wavelength shows that the bedforms with the shortest wavelength are found in areas with the steepest slopes, and the bedforms with the longest wavelength occur in areas where the gradient is least steep (Fig. 11C). The observed distal increase in bedform wavelength is inconsistent with an interpretation of the bedforms as antidunes. If the bedforms were antidunes, the balance described by Equation 5 would suggest that their wavelength would be expected to decrease, rather than increase, as a result of diminished velocity and excess density toward the distal part of the bedform field.

Cyclic steps produced by density currents in the laboratory are typically built from plastic particles with a settling velocity equivalent to fine sand (e.g., Spinewine et al. 2009; Kostic et al. 2010), or from fine sand itself (e.g., Cartigny 2012). These experimental sediment types have a narrow range of grain sizes, in which the sediment particles act as bedload, and a saline solution is used as a proxy for the fine particles that would serve to increase density in a natural flow. The sediment mixture used in the experiments of Spinewine et al. (2009) has a very narrow grain-size distribution; nonetheless the authors observe downstream fining of the deposited material. The range of grain sizes in the Stehekin delta system spans three orders of magnitude from coarse sand through clay. In this natural environment, distal deposition of sand occurs primarily within the bedform field, where hyperpycnal flow velocities are sufficiently elevated to transport sand. The silt and clay fraction carried during hyperpycnal flows fines laterally away from the high-velocity bedform field, as well as distally down the axis of the lake toward the south. Such planform descriptions of cyclic steps have no counterpart in the experimental literature because of the laterally confined flumes in which cyclic steps have so far been studied. In order to understand the signatures of cyclic steps in an unconfined natural system, we must connect the processes acting within the bedform field to the fluvial source of the hyperpycnal flows.

Relating Sedimentary Signatures to Fluvial Processes

Signals from the Stehekin River.—Data from the Stehekin River are limited to measurements of water discharge just upstream of Lake Chelan (USGS gauge #12451000), and 11 measurements of suspended-sediment concentration at the same site (Nelson 1973). A suspended-sediment discharge of $\sim 5700 \text{ m}^3 \text{ y}^{-1}$ was estimated from these water samples collected in the lowermost Stehekin River (Nelson 1973). However, the suspended-sediment rating curve from which this value was determined, only includes data from flows below $\sim 200 \text{ m}^3 \text{ s}^{-1}$, roughly four times less than the peak discharge. Consequently, sediment discharge during flood events, which likely dominates the delivery of sediment to Lake Chelan, remains poorly constrained. A second estimate of sediment deposited in the most proximal delta over the last 9000 years reveals an average sediment discharge of $\sim 19,000 \text{ m}^3 \text{ y}^{-1}$, although this value likely underestimates the amount of fine sediment carried in suspension and deposited in deep water (Riedel 2008). However, this value also integrates over a time period that includes extensive alpine deglaciation following the last glacial maximum, and may therefore overestimate the volume of sediment discharged in modern times.

Using the ^{210}Pb sediment accumulation rates calculated from five cores collected on the subaqueous Stehekin delta (Fig. 9), it is possible to construct a rough sediment budget for the survey area. The sediment budget is based on a simplified pattern of sediment accumulation within the survey area. Sediment accumulation is defined to be 5 mm y^{-1} at the proximal edge of the delta, and to diminish linearly, reaching a value of 2 mm y^{-1} along the distal edge of the survey area. In most depositional systems, especially those as quiescent as Lake Chelan, sediment accumulation is greatest nearest the sediment source, and decreases distally, a pattern consistent with the bathymetry of the delta slope within the survey area (e.g., Desloges and Gilbert 1994). Because the basin is very narrow, and because CHIRP cross sections show sediment accumulation over the full basin width (excluding steep bedrock basin walls), the simplified geometry assumes equal rates of sediment accumulation across the lake. This simplified geometry suggests an average of $\sim 9000 \text{ m}^3$ of sediment accumulates in the study area annually. The yearly accumulation calculated here falls between the two estimates of sediment discharge reported in Nelson (1973) and Riedel (2008) (5700 m^3 and $19,000 \text{ m}^3$, respectively).

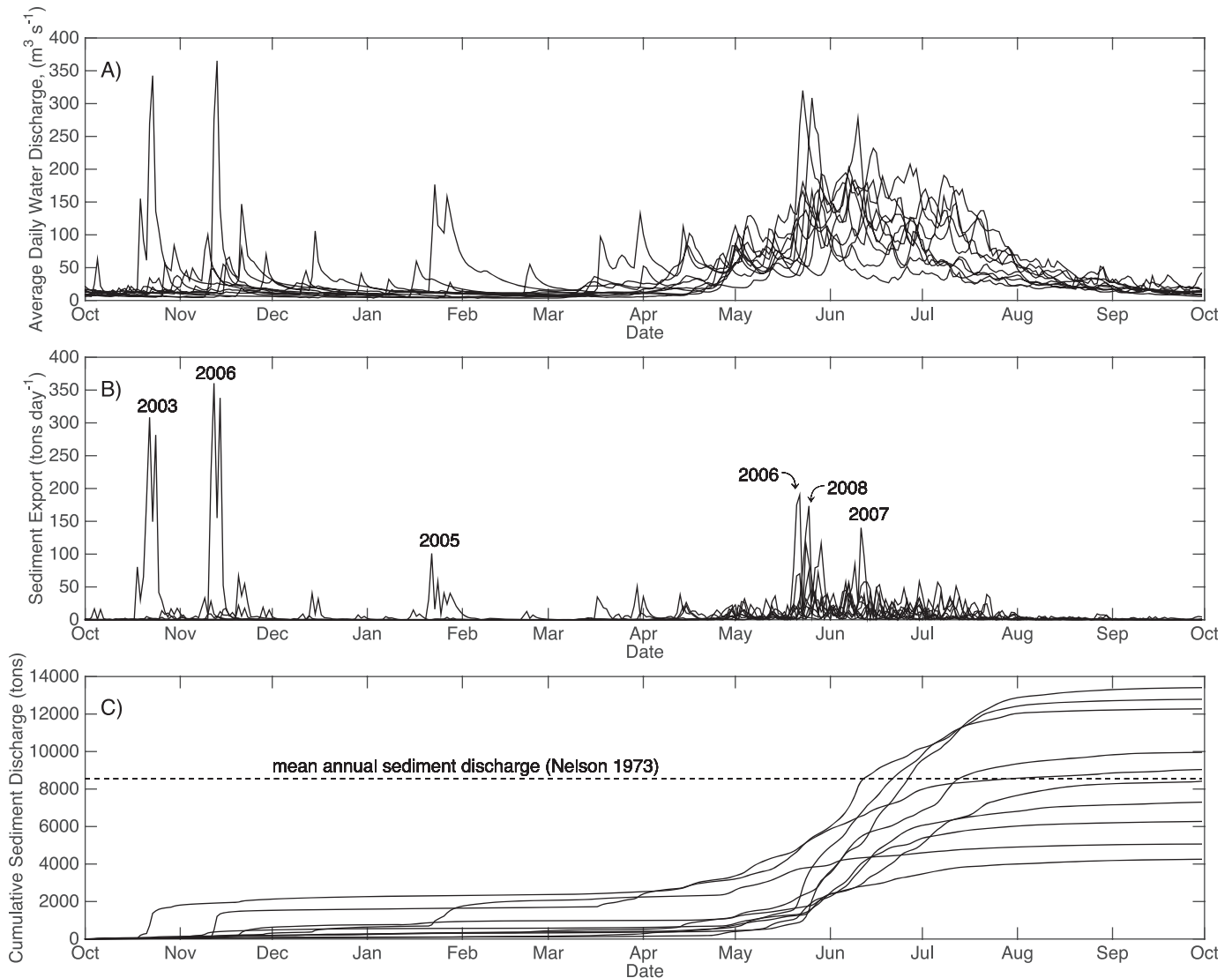


FIG. 12.—Time series of water discharge and suspended-sediment export from the Stehekin River for water years 2001–2010. **A)** Average daily water discharge ($\text{m}^3 \text{s}^{-1}$) measured at USGS gauge #12451000 on the lower Stehekin River. **B)** Daily sediment export from the Stehekin River based on the water discharge data shown in Part A and a standard rating curve calculated as a linear regression through log-transformed measurements of suspended-sediment concentration and water discharge from Nelson (1973). Major discharge events are marked by calendar year of occurrence. **C)** Cumulative annual sediment discharge of the Stehekin River. Note the stereotyped shape of the curves associated with late-fall storms and spring snow melt. The dashed line marks the average annual suspended-sediment discharge reported by Nelson (1973) of 5700 m^3 or $\sim 8550 \text{ kg}$, assuming a sediment bulk density of 1500 kg m^{-3} .

Although a rating curve based on the 11 suspended-sediment-concentration values from Nelson (1973) is only a first-order approximation of the sediment-discharge behavior of the Stehekin River, it highlights the important contribution of intense, short-lived discharge events to the cumulative annual discharge of sediment (Fig. 12). This rating curve is calculated as a linear regression through log-transformed measurements of suspended-sediment concentration and water discharge:

$$\log(C) = b \log(Q) + \log(a) \quad (6)$$

where C is suspended-sediment concentration, Q is water discharge, and a and b are the intercept and slope of the linear regression, respectively (after Syvitski et al. 2000). This relationship can also be written in the more common power-law formulation:

$$C = aQ^b \quad (7)$$

Applying this rating curve to ten years of water-discharge data up to and including the study period (water years 2001–2010), illustrates the importance of short-lived flood events to the export of sediment from the Stehekin River to Lake Chelan on daily and annual timescales (Fig. 12). The contribution of these flood events can be seen both as peaks in daily sediment flux (Fig. 12B), as well as nearly stepwise increases in the cumulative sediment discharge curves (Fig. 12C). The peak in suspended-sediment export in May 2006 corresponds to the flood and hyperpycnal flow shown in Figure 1. While we are unable to say which peaks in sediment export produce hyperpycnal flows, 10 years of data (Fig. 12) include four peaks of a similar or larger magnitude than the May 2006 peak, suggesting hyperpycnal flows of this scale may occur on average every 2–3 years in this system. The duration of high-discharge events is similar between years, with each lasting 3–5 days. Even if a strongly plunging flow lasts for only a portion of each high-discharge period, such flows would be classed as sustained hyperpycnal flows as

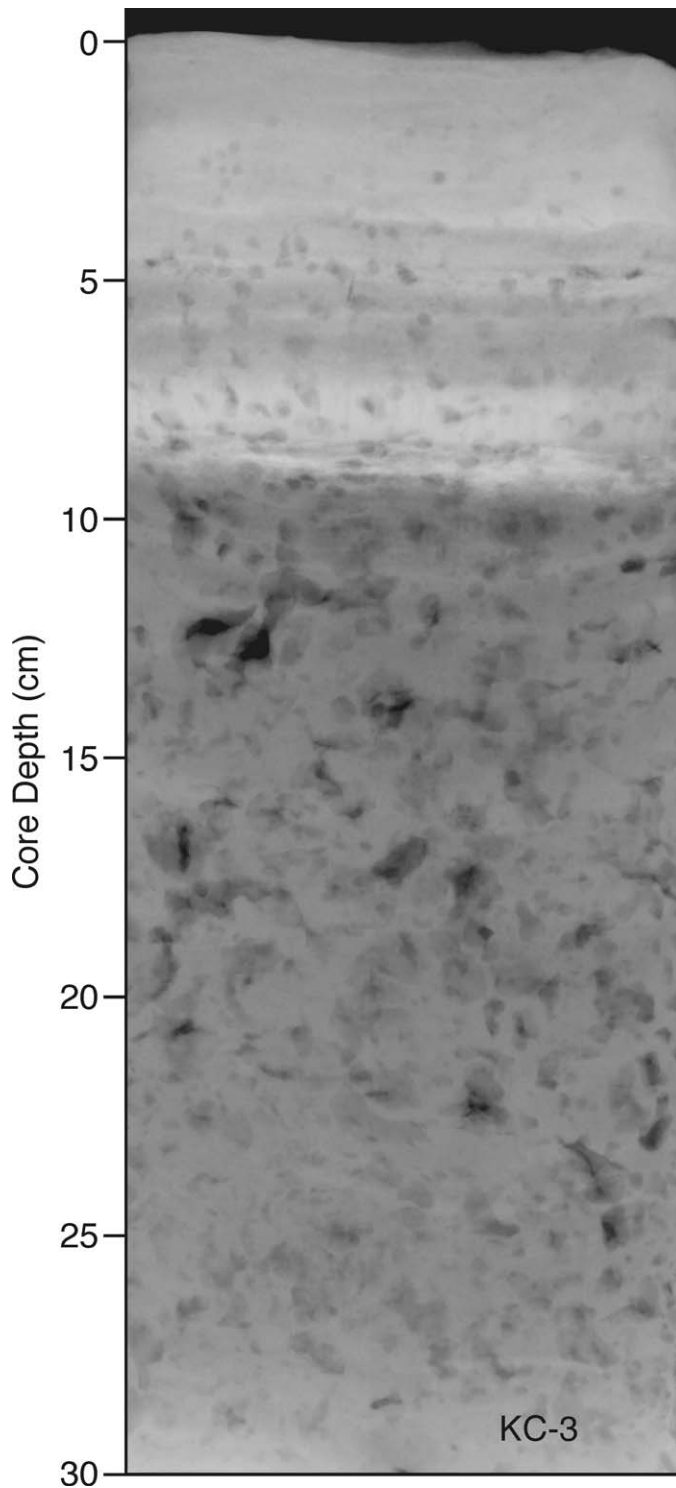


FIG. 13.—X-radiograph negative of the upper 30 cm of core KC-3 collected ~ 2500 m from the delta rollover at a water depth of ~ 150 m (Fig. 4). Dark spots in the image are due to pockets of biogenic gas in the sediment. The upper 8 cm of the core is physically stratified and corresponds to the region of constant ^{210}Pb excess activity. All five cores exhibit similar patterns in physical structure and ^{210}Pb excess activity (Fig. 9).

opposed to surge-type flows. The duration of surge-type flows, often the product of submarine slope failures, is usually measured in minutes (Mulder et al. 2003). This difference in duration between surge-type flows and longer-duration, or sustained flows, impacts the character of the resultant sedimentary deposits.

Signals Preserved in Sediments.—In addition to forming cyclic steps along their flow path, hyperpycnal flows originating from the Stehekin River leave a signature outside the bedform field. Profiles of excess ^{210}Pb show a zone (~ 10 cm thick) of constant activity at the top of each core (Fig. 9). While this closely resembles a surface mixed layer (e.g., Nittrouer et al. 1979), X-radiographs of cores show no evidence of bioturbation (Fig. 13). Such layers may record single events such as a large flood of the Stehekin River, like that which occurred in 2006. Other low-frequency events, such as landslides and temporarily increased sediment yield due to forest fires, may also produce sediment-laden discharges capable of plunging and creating the bedforms observed in the study area.

Most density-driven flows can be divided into a head, a body, and a tail. In a sustained density current, the passing of the turbulent head of the flow represents a small fraction of the total flow duration. In such a flow, the long-duration, relatively stable body of the flow dominates the sedimentary signature left by passing current. In a surge-type flow, the turbulent head of the flow represents a larger proportion of the flow duration and likely dictates the character of the resultant morphology (Lamb et al. 2004). The spatial distribution of grain sizes on the Stehekin delta indicates strong lateral shear between the flow and the ambient lake water. Approximately 1 km from the topset, hyperpycnal flows moving downslope remain sufficiently focused to deposit fine sand along the axis of the bedform field (> 80% sand, Fig. 7), and much finer sediment less than 150 m to the side (i.e., <50% sand in KC6, Fig. 8). In addition to changes in grain size, the focused nature of these flows is captured in the CHIRP data as a sharp transition between the coarser, acoustically structureless sediments within the bedform field, and finer flat-lying laminated sediments on either side (Fig. 14).

The focused character of the hyperpycnal flows on the Stehekin delta may result from their long duration, like the sustained turbidity currents described in experiments by Alexander et al. (2008). While these experimental flows were subcritical, the authors argue that sustained turbidity currents exhibit limited lateral expansion, due to the dominance of vertical turbulent momentum exchange (Alexander et al. 2008). In contrast, the deposits associated with surge-type turbidity currents tend to be more fan-like, the result of predominantly lateral momentum exchange. The hydraulic jump associated with a cyclic step, in which kinetic energy is exchanged for potential energy in a turbulent vertical jump, is an efficient mechanism for vertical turbulent momentum exchange (Long et al. 1991; Kostic and Parker 2006). On the Stehekin delta, the combination of sustained flows and cyclic hydraulic jumps appears to promote strong focusing of the flow, resulting in a narrow band of bedforms, sharp lateral gradients in grain size and bedding character, and locally elevated bathymetry within the bedform field. In essence, the development of stable hydraulic jumps appears to promote vertical mixing at the expense of lateral mixing, resulting in self-confinement of these hyperpycnal flows. Perhaps this aspect of cyclic-step morphology has so far gone unnoticed because depositional cyclic steps have primarily been studied in laterally confined flumes where this behavior would not be observable (e.g., Winterwerp et al. 1992; Taki and Parker 2005; Sun and Parker 2005; Kostic and Parker 2006; Cartigny et al. 2011, 2014).

CONCLUSIONS

Evidence of hyperpycnal flows from the Stehekin River is preserved in a kilometer-scale train of bedforms on the foreset of the Stehekin River delta. An analysis of the characteristics of these bedforms, and the

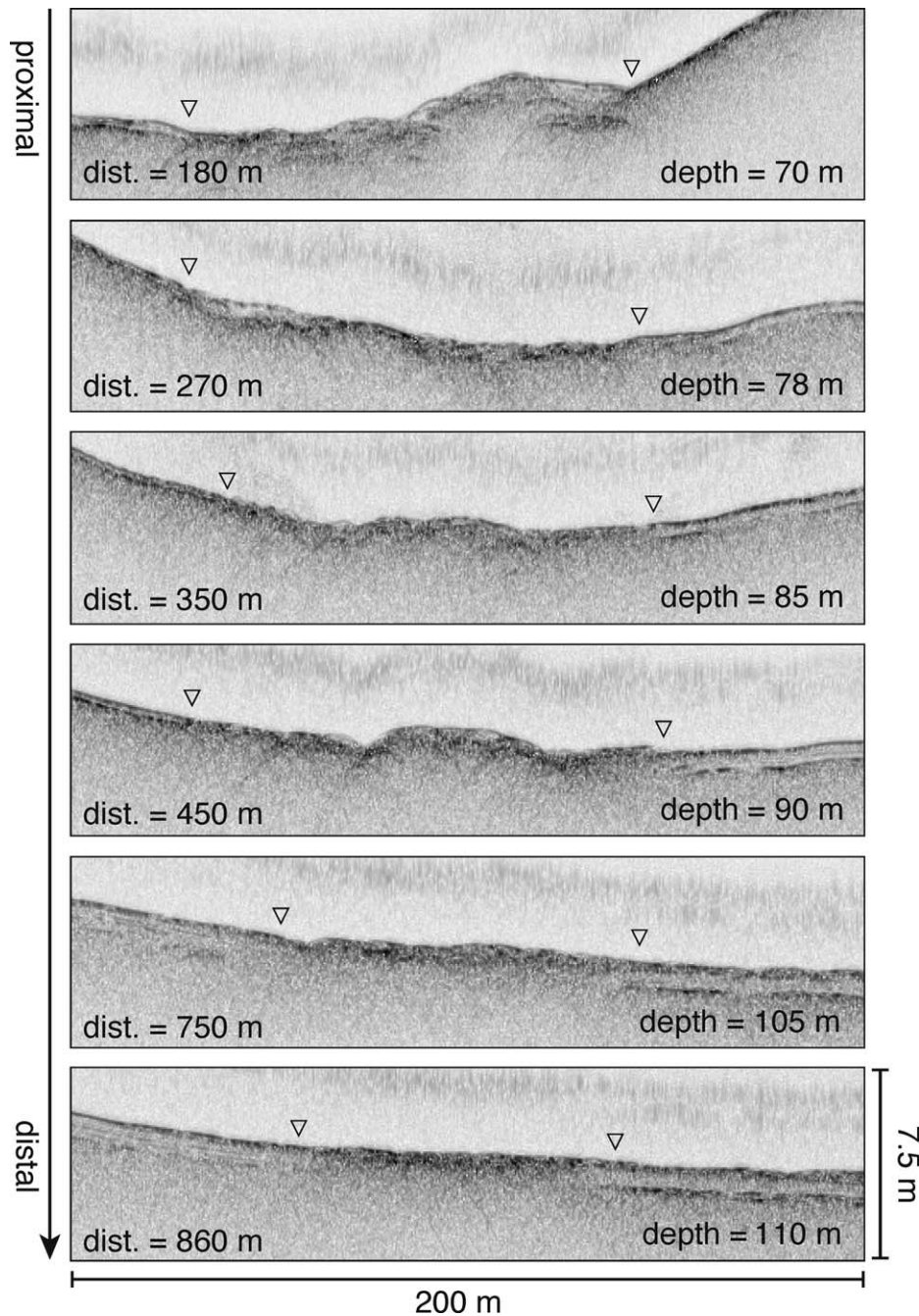


FIG. 14.—CHIRP cross sections through the bedform field at six locations between 70 and 860 m from the delta rollover. Each cross section is nearly perpendicular to the trend of the bedform field and is displayed at the same scale (200 m \times 7.5 m). The cross sections are arranged from most proximal (top) to most distal (bottom). Triangles mark the approximate location of the transition between the bedform field and lateral flat-lying sediments with parallel reflectors.

hyperpycnal fluvial discharges that created them, supports the following conclusions:

1. Hyperpycnal discharges of the Stehekin River are supercritical ($Fr_d > 1$). This is due to the steep slope of the foreset ($\sim 3\text{--}7^\circ$), and the reduced gravity condition of two-layer flows relative to subaerial flows.
2. The bedforms on the foreset of the Stehekin Delta are cyclic steps. An interpretation of the bedforms as antidunes is rejected because the wave speed of the upstream-propagating interfacial wave, with which antidunes would necessarily be in phase, would be too slow to balance the high downstream velocity (due to steep bed slope) of the hyperpycnal flow. The trend of increasing bedform wavelength toward the distal end of the system is consistent with the

interpretation of the bedforms as cyclic steps, and inconsistent with antidunes.

3. The linear nature of the bedform field, and associated sharp lateral gradients in grain size and bedding character, are promoted by the presence of hydraulic jumps and the sustained nature of the hyperpycnal flows. Hydraulic jumps serve to limit lateral momentum exchange by promoting vertical momentum exchange. Sustained flows are dominated by the stable body of the flow and minimize the signature of the turbulent head of the flow.
4. The cyclic steps on the Stehekin delta foreset are formed by bottom-hugging hyperpycnal discharges of the Stehekin River. These flows likely occur during short-lived high-discharge events during which sediment export from the Stehekin River is highest. During these

events, the excess density of the Stehekin River discharge is sufficient to cause the river outflow to plunge and sculpt the bed into a series of cyclic steps.

Previous studies have described cyclic steps that are approximately two orders of magnitude larger than those in Lake Chelan and are associated with submarine canyons (Fildani et al. 2006; Lamb et al. 2008). The depositional cyclic steps described here bridge the gap between those large field examples and the sub-meter-scale cyclic steps characterized by laboratory experiments (Winterwerp et al. 1992; Kostic et al. 2010; Cartigny 2012). Experimental cyclic steps produced in narrow flumes are unable to resolve the planform geometry of the sedimentary bodies produced by unconfined Froude-supercritical flows, like those in Lake Chelan. Further observations are needed to fully describe the hydrodynamic mechanisms that produce the elongate, nonchannelized bedform field observed in Lake Chelan. The flow dynamics and depositional patterns described here are likely applicable to other lacustrine systems, and to marine environments where sustained Froude-supercritical density currents are likely to occur, including the continental slope during sea-level lowstands.

ACKNOWLEDGMENTS

This study was made possible through cooperation with the National Park Service. The Royalty Research Fund of the University of Washington provided significant funding for this project. Rip Hale, Kyle Womack, Kerrie Sampelayo, Jim Shobe, Kieran Dunne, Dan Nowacki, Katie Boldt, Kristen Webster, and Miles Logsdon provided excellent field and lab assistance. Comments from John Swenson, Paul Myrow, and two anonymous reviewers improved an earlier version of this paper. We thank the University of Texas Institute for Geophysics, who provided help with R/V Itasca logistics.

REFERENCES

- ALEXANDER, J., McLELLAND, S.J., GRAY, T.E., VINCENT, C.E., LEEDER, M.R., AND ELLETT, S., 2008, Laboratory sustained turbidity currents form elongate ridges at channel mouths: *Sedimentology*, v. 55, p. 845–868.
- ASHLEY, G., 1990, Classification of large-scale subaqueous bedforms: a new look at an old problem: *Journal of Sedimentary Petrology*, v. 60, p. 160–172.
- CARTIGNY, M., 2012, Morphodynamics of Supercritical High-Density Turbidity Currents: *Utrecht Studies in Earth Sciences*, 153 p.
- CARTIGNY, M., POSTMA, G., AND VAN DEN BERG, J., 2011, A comparative study of sediment waves and cyclic steps based on geometries, internal structures and numerical modeling: *Marine Geology*, v. 280, p. 40–56.
- CARTIGNY, M., VENTRA, D., POSTMA, G., AND VAN DEN BERG, J., 2014, Morphodynamics and sedimentary structures of bedforms under supercritical-flow conditions: new insights from flume experiments: *Sedimentology*, v. 61, p. 712–748.
- COVAULT, J.A., KOSTIC, S., PAULL, C.K., RYAN, H.F., AND FILDANI, A., 2014, Submarine channel initiation, filling and maintenance from sea-floor geomorphology and morphodynamic modelling of cyclic steps: *Sedimentology*, v. 61, p. 1031–1054.
- DESLOGES, J.R., AND GILBERT, R., 1994, Sediment source and hydroclimatic inferences from glacial lake sediments: the postglacial sedimentary record of Lillooet Lake, British Columbia: *Journal of Hydrology*, v. 159, p. 375–393.
- FILDANI, A., NORMARK, W.R., KOSTIC, S., AND PARKER, G., 2006, Channel formation by flow stripping: large-scale scour features along the Monterey East Channel and their relation to sediment waves: *Sedimentology*, v. 74, p. 148–155.
- HAND, B.M., 1974, Supercritical flow in density currents: *Journal of Sedimentary Petrology*, v. 3, p. 637–648.
- KENNEDY, J.F., 1963, The mechanics of dunes and antidunes in erodible-bed channels: *Journal of Fluid Mechanics*, v. 16, p. 521–544.
- KNELLER, B., AND BUCKEE, C., 2000, The structure and fluid mechanics of turbidity currents: a review of some recent studies and their geological implications: *Sedimentology*, v. 47, p. 62–94.
- KOSTIC, S., 2011, Modeling of submarine cyclic steps: controls on their formation, migration, and architecture: *Geosphere*, v. 7, p. 294–304.
- KOSTIC, S., AND PARKER, G., 2006, The response of turbidity currents to a canyon-fan transition: internal hydraulic jumps and depositional signatures: *Journal of Hydraulic Research*, v. 44, p. 631–653.
- KOSTIC, S., SEQUEIROS, O., SPINOWINE, B., AND PARKER, G., 2010, Cyclic steps: a phenomenon of supercritical shallow flow from the high mountains to the bottom of the ocean: *Journal of Hydro-environment Research*, v. 34, p. 167–172.
- KUEHL, S.A., NITTROUER, C.A., DEMASTER, D.J., AND CURTIN, T.B., 1985, A long, square-barrel gravity corer for sedimentological and geochemical investigation of fine-grained sediments: *Marine Geology*, v. 62, p. 365–370.
- LAMB, M.P., HICKSON, T., MARR, J.G., SHEETS, B., PAOLA, C., AND PARKER, G., 2004, Surging versus continuous turbidity currents: flow dynamics and deposits in an experimental intraslope minibasin: *Journal of Sedimentary Research*, v. 74, p. 148–155.
- LAMB, M.P., PARSONS, J.D., MULLENBACH, B.L., FINLAYSON, D.P., ORANGE, D.L., AND NITTROUER, C.A., 2008, Evidence for super-elevation, channel incision, and formation of cyclic steps by turbidity currents in Eel Canyon, California: *Geological Society of America, Bulletin*, v. 120, p. 463–475.
- LEE, H., SYVITSKI, J.P.M., PARKER, G., ORANGE, D., AND LOCAT, J., 2002, Distinguishing sediment waves from slope failure deposits: field examples, including the “Humboldt slide,” and modelling results: *Marine Geology*, v. 192, p. 79–104.
- LONG, D., RAJARATNAM, N., STEFFLER, P.M., AND SMY, P.R., 1991, Structure of flow in hydraulic jumps: *Journal of Hydraulic Research*, v. 29, p. 207–218.
- MIDDLETON, G., AND SOUTHWARD, J., 1984, *Mechanics of Sediment Movement: SEPM, Short Course Notes*, no. 3.
- MULDER, T., SYVITSKI, J.P.M., MIGEON, S., FAUGERES, J., AND SAVOYE, B., 2003, Marine hyperpycnal flows: initiation, behavior and related deposits. A review: *Marine and Petroleum Geology*, v. 20, p. 861–882.
- NELSON, L., 1973, Sediment transport by streams in the Upper Columbia River Basin, Washington, May 1969–June 1971: U.S. Geological Survey, Water Resources Division. Water-Resources Investigations 39-73.
- NITTROUER, C.A., STERNBERG, R.W., CARPENTER, R., AND BENNETT, J.T., 1979, Use of Pb²¹⁰ geochronology as a sedimentological tool: application to the Washington continental shelf: *Marine Geology*, v. 31, p. 297–316.
- PARKER, G., 1996, Some speculations on the relation between channel morphology and channel-scale flow structures, in Ashworth, P., Bennett, S., Best, J., and McLelland, S., eds., *Coherent Flow Structures in Open Channels*: New York, John Wiley & Sons, p. 423–458.
- PELLETIER, G., PATMONT, C., WELCH, E., AND BANDON, D., 1989, Lake Chelan Water Quality Assessment: Washington State Department of Ecology, 434 p.
- RIEDEL, J., 2008, White paper #1, Stehekin River Corridor Implementation Plan: National Park Service, 43 p.
- SPINOWINE, B., SEQUEIROS, O.E., GARCIA, M.H., BEAUBOUF, R.T., SUN, T., SAVOYE, B., AND PARKER, G., 2009, Experiments on wedge-shaped deep sea sedimentary deposits in minibasins and/or on channel levees emplaced by turbidity currents. Part II. Morphodynamic evolution of the wedge and of the associated bedforms: *Journal of Sedimentary Research*, v. 79, p. 608–628.
- SUN, T., AND PARKER, G., 2005, Transportational cyclic steps created by flow over an erodible bed. Part 2. Theory and numerical simulation: *Journal of Hydraulic Research*, v. 43, p. 502–514.
- SYVITSKI, J.P.M., MOREHEAD, M.D., BAHR, D.B., AND MULDER, T., 2000, Estimating fluvial sediment transport: the rating parameters: *Water Resources Research*, v. 36, p. 2747–2760.
- TAKI, K., AND PARKER, G., 2005, Transportational cyclic steps created by flow over an erodible bed. Part 1. Experiments: *Journal of Hydraulic Research*, v. 43, p. 488–501.
- WHETTEN, J.T., 1967, Lake Chelan Washington: bottom and sub-bottom topography: *Limnology and Oceanography*, v. 12, p. 253–259.
- WINTERWERP, J.C., BAKKER, W.T., MASTBERGEN, D.R., AND VAN ROSSUM, H., 1992, Hyperconcentrated sand–water mixture flows over erodible bed: *Journal of Hydraulic Engineering*, v. 118, p. 1508–1525.

Received 18 July 2014; accepted 23 March 2015.